UDC 551.558.1:551.513.1

VORTEX FORMATION BY SUCCESSIVE THERMALS: A NUMERICAL SIMULATION

EUGENE M. WILKINS,[1] YOSHIKAZU SASAKI, and ROGER H. SCHAUSS
University of Oklahoma, Norman, Okla.

ABSTRACT

The purpose of this research is to investigate, by means of numerical simulation experiments, the complex interactions between consecutive toroidally circulating buoyant elements (thermals) when these occur in either rotating or nonrotating environments. The study includes both the vortex formation process and the effect that this process has on the properties of the one or more buoyant elements involved in the interaction.

A numerical model of a self-developing thermal of the Ogura type was modified to include tangential accelerations and a provision for injecting a second thermal into the field of a previous one. Computer outputs are obtained at several times during the evolution of both solitary thermals and two types of successive thermals, released at intervals of 2 and 7 min. These were also performed for three different magnitudes of pre-existing vorticity, comparable to magnitudes measured in the vicinity of thunderstorms. The results of the complex interactions are illustrated in the patterns of isotherms, stream functions, and velocity isotachs.

A thermal is accelerated in circulation and velocity of rise upon encountering the wake of a previous thermal, and velocity enhancements can be quite spectacular. A rotation field causes both solitary and successive thermals to surrender part of their kinetic energy to vortex formation, but lateral confinement of the thermal slows the mixing and reduces the heat loss. The first effect tends to suppress the vertical momentum of the thermal, and the second one tends to enhance it. Nevertheless, all but one of the solitary and successive thermals investigated were suppressed by the vortex formation interaction; this one, a second thermal with a 7-min interval, appears to represent an optimum combination of buoyancy and ambient vorticity, since it forms a more intense vortex and simultaneously maintains the strongest vertical velocity for one particular magnitude of ambient vorticity. When the rotation rate initially is very large, on the other hand, a solitary thermal is "dominated" by the rotation field, and neither forms a strong vortex nor develops the usual characteristics of a vigorous thermal.

The results show several features of the numerical simulation to be in agreement with solitary and successive thermals simulated in the laboratory. Some possible recognition features are suggested for the detection of situations where strong interactions occur between a buoyant element and the ambient vorticity field. Some of the results must be applicable to atmospheric convection. The computations relating to vortex formation must be considered relevant to tornadoes, despite the shallow depth used for the convection layer.

1. INTRODUCTION

The subject of interacting successive thermals apparently has received little attention from meteorologists, even though the phenomenon may very well occur in convection as an important transition stage between sporadic solitary thermals and continuous plumes. In our present state of knowledge, it is even uncertain whether the study of successive thermals is more appropriately concerned with weak dry convection or with buoyant elements on the scale of those involved with severe storms. It is fairly common to see thermals of the heavy cumulus type treated mathematically as discrete elements; and very recently, Warner and Telford (1967) investigated clear-air convection that seemed to them to consist exclusively of continuous plumes. Ludlum (1964) considered a thunderstorm model that involves a succession of individual convective elements growing in the updraft of the storm.

If successive thermals may become volved in thunderstorms, they may also be active in the concentration of vorticity. The rotation of severe storm regions about some vertical axis has been observed in time-lapse films of radar PPI-scope (plan position indicator) presentations (e.g., Fujita et al. 1966). Williams (1962) found that regions in the vicinity of thunderstorms often are characterized by rather large values of the vertical component of vorticity, say, 10^{-3} s^{-1} or greater. This is of the same order as the vorticity selected as an ambient condition for the environment into which our simulated thermals are injected. Giles (1967) investigated several storms that occurred within the Beta Network of the National Severe Storms Laboratory and found that some of the most severe of the storms were associated with mesoscale regions of cyclonic vorticity.

There is some satisfaction in the knowledge that the phenomena we have chosen to simulate *could* occur in nature and even more satisfaction in the strong suspicion that such processes do occur, at least occasionally. Knowledge as to whether successive thermal interactions are sufficiently frequent as to be of major importance may be some time in coming. Meanwhile, these investigations are felt to be justified on the grounds that the simulations may reveal certain recognition features that would become important in determining when and if such phenomena do occur in nature. It turns out that not all of the results of these simulations can be predicted intuitively. When vortex formation occurs, a solitary thermal stretches vertically to such an extent that it may give the appearance of a continuous plume; and this may make discrimination rather difficult. The updraft in the wake between successive

[1] Also at the LTV (Ling-Temco-Vought, Inc.) Research Center, Dallas, Tex.

thermals could also give the appearance of a plume for any observational techniques presently available.

To the best of our knowledge, this is the first research project to be concerned with:

1. The interactions of successive thermals with each other,
2. The interactions of solitary and successive discrete thermals with a rotation field, and
3. The effect on the thermal itself of partitioning its energy into a tangential velocity field as well as into its own toroidal circulation and velocity of rise.

Attention in the past has been focused on either solitary thermals in a nonrotating medium or vortex formation due to a steady sink in a rotating fluid. The first of these has been modeled in the laboratory by Scorer (1957), Woodward (1959), Richards (1961), and Turner (1963), and numerically by Malkus and Witt (1959), Ogura (1962, 1963), and Lilly (1962, 1964, 1965). The second phenomenon has received considerably more attention in both theory and laboratory experiment; the classical works by Long (1956, 1958, 1961), Morton (1963), and Turner and Lilly (1963) are cited as examples. All of these works have made important contributions to our knowledge about convection and vortex formation as entirely separate entities.

The subject of cellular convection in a rotating fluid has been treated extensively from the fluid mechanics viewpoint. The classical predictions in theory by Chandrasekhar (1953) and Veronis (1959) of cellular flow patterns and critical Rayleigh numbers for the onset of convection have been verified experimentally by Nakagawa and Frenzen (1955), Fultz and Nakagawa (1955), Dropkin and Globe (1959), and Goroff (1960). A comprehensive summary on this subject has been given by Chandrasekhar (1961). The results of the cellular convection studies are related to this study mainly in the suppression of the convection by rotation.

In addition to these works, our thinking about convective vortexes has also been influenced by Kuo (1966) who gave special emphasis to the importance of the pre-existing ambient vorticity of the kind measured by Williams (1962) and Giles (1967). Kuo states that this vorticity not only becomes concentrated within the convective cell owing to its being drawn inward from the cell's effective radius but also that the vorticity restrains the growth of the effective radius by acting as a magnified Coriolis force. We find this to be indicated in both the laboratory simulations and the computer simulations.

The first experiments on this project (Wilkins et al. 1969) consisted of laboratory simulations of adiabatic and nonadiabatic thermals in a rotating tank of fluid. The equations of Morton et al. (1956), expressing the conservation of volume, density deficit, and vertical momentum, were modified to take into account the production of buoyancy within the cloud and also the vertical acceleration on the cloud due to its interaction with a rotating medium. This acceleration term, which was added to the momentum conservation equation, was derived with the assumption that kinetic energy and angular momentum are conserved in the environmental fluid which is pulled radially inward toward the base of the rising thermal. The only parameters that could be measured quantitatively in the laboratory experiments were the cloud volume and the height of rise of the thermal cap, at various time intervals. These were obtained by a photogrammetric technique. The agreement between theory and experiment is fair, but the prediction of the rotation effect depends upon the effective radius of the thermal. This could only be estimated crudely. The agreement was considerably better for the nonrotation experiments, however, whether the simulated clouds were nonadiabatic or adiabatic.

In a parallel effort, Inman (1966) solved a numerical model for convection in a rotating medium. This model, patterned after Ogura (1963), is more appropriate for the atmosphere than was the previous one. The model was subsequently improved by Friday (1969) and has been extended to the simulation of consecutive thermals in this paper. The Ogura model is excellent for analyses of this kind; and Ogura (1962) showed that, in addition, the thermal behaves as predicted by similarity theory and as observed in the tank experiments.

Consecutive thermal simulations were also conducted in the laboratory thermal tank by Wilkins et al. (1971), and some significant results were obtained despite considerable experimental difficulties. The second buoyant cloud overtakes the first one and is very soon obscured by it. We are now trying to develop a slower rising thermal to allow a longer time interval between thermals. Also, the initial thermal will be made transparent so that the effect of its wake on a subsequent thermal can be measured without obscuration. The model based on the conservation equations was modified still further to take into account a wake velocity residual from a preceding thermal. The agreement with the experimental data is fair for a reasonable selection of parameters, but a longer thermal lifetime for second and subsequent thermals is needed to make a more suitable test of the theory.

The fact that we dare to attack the immensely complex problem of consecutive thermals in a rotating environment seems to imply a considerable amount of knowledge about the subject. This is regrettable and completely misleading. The authors confess to a great amount of ignorance about the even simpler (though still complex) phenomena such as solitary thermals in a rotating fluid, consecutive thermals in a nonrotating fluid, and for that matter, solitary thermals in a stationary fluid. The apparent giant step came about as a result of some numerical techniques that were a fallout from research on a different problem. The salient feature of Ogura's self-developing thermal is that we are enabled to observe the effects of some complex interactions without the necessity for presuppositions on our part. Thus, we are

emboldened to proceed, more due to the possession of a powerful analysis tool than by any special knowledge on our part. It is hoped that parallel studies with laboratory simulations and simpler mathematical models will improve our understanding.

Several simplifications have been made in the numerical model that must be regarded as departures from circumstances peculiar to real atmospheric thermals. The major simplifications are:

1. The thermals are axially symmetric.
2. First and succeeding thermals originate from the same point and follow the same path.
3. First and succeeding thermals have the same buoyancy initially, and buoyancy is invariant with time.
4. The treatment considers only the first two thermals in a series.

Since the model is only 4 km in depth, we cannot simulate thermals far enough apart so as not to interact strongly, and yet even the effects of residual turbulence from a relatively old wake may be of considerable importance to the study of atmospheric thermals. Probably there are also important interactions between thermals that do not follow the same vertical path. Furthermore, third and subsequent thermals, if they happen to follow the same path, may behave in a much different manner from those of the first two in the series. However, we need not concern ourselves with all of the neglected processes to study some of the effects of vortex formation by solitary and succesive thermals.

2. METHOD

The set of dynamic equations used in the numerical simulation is patterned after the set introduced by Ogura and Phillips (1962) and subsequently used in the modeling of both dry and moist convection by Ogura (1962, 1963). This model was further modified by Inman (1966) to account for tangential motions. The new terms are eq (2) and the fourth term on the right side of eq (1). The equations are written in cylindrical coordinates as

$$\frac{\partial u}{\partial t}=-u\frac{\partial u}{\partial r}-w\frac{\partial u}{\partial z}-c_p\Theta\frac{\partial \pi'}{\partial r}+\frac{v^2}{r}+\kappa\left(\nabla^2 u-\frac{u}{r^2}\right), \quad (1)$$

$$\frac{\partial v}{\partial t}=-u\frac{\partial v}{\partial r}-w\frac{\partial v}{\partial z}-\frac{uv}{r}+\kappa\left(\nabla^2 v-\frac{v}{r^2}\right), \quad (2)$$

$$\frac{\partial w}{\partial t}=-u\frac{\partial w}{\partial r}-w\frac{\partial w}{\partial z}-c_p\Theta\frac{\partial \pi'}{\partial z}+\kappa\nabla^2 w+\frac{g\theta'}{\Theta}, \quad (3)$$

$$\frac{\partial \phi'}{\partial t}=-u\frac{\partial \phi'}{\partial r}-w\frac{\partial \phi'}{\partial z}+\kappa\nabla^2\phi', \quad (4)$$

and

$$\frac{\partial (ru)}{\partial r}+\frac{\partial (rw)}{\partial z}=0. \quad (5)$$

The velocity components; u, v, and w are radial, tangential, and vertical, respectively; c_p is the specific heat at constant pressure; $c_p\phi'$ is the anomaly of specific entropy from a dry adiabatic atmosphere; g is gravitational acceleration; and κ is a constant coefficient of eddy viscosity. The nondimensional variable π is given by

$$\pi=(p/P)^{R/c_p} \quad (6)$$

where p is pressure, $P=1000$ mb, R is the gas constant for dry air, and π' represents the deviation of π from that of a dry isentropic atmosphere of constant potential temperature Θ. In the original model, the anomaly ϕ' was generated by simulation of the latent heat of condensation; and the same plan was followed in the computations by Inman (1966). A further modification by Friday (1969) simplified this nonadiabatic effect by means of a buoyancy production term based on a fixed percentage of the value of ϕ' existing at the time. Numerical simulations of thermals conducted by Friday showed that the same general conclusions could be drawn about the vortex formation interactions whether the thermals were adiabatic or nonadiabatic; consequently, only constant buoyancy thermals have been used throughout this study. Continuity of buoyancy production is not equivalent to continuity of sink in the case of a discrete buoyant element, and thus the interaction of the thermal with the rotation field is a nonsteady process regardless of buoyancy production.

Ogura (1962) found that the grid introduces an effect similar to that of an eddy viscosity. It tends to mask the real eddy viscosity even when values of κ as great as 4×10^5 cm$^2\cdot$s^{-1} are used. Inman (1966) obtained a similar result with the computational scheme used on this project. For this reason, the Reynolds stress terms were dropped from the governing equations.

The boundary conditions and the method of initialization of the self-evolving thermal by introduction of a distribution of temperature anomaly θ' are similar to those of Ogura (1962). The temperature distribution initially is

$$\theta'(r,z)=\theta_0\sin^2(\pi z/600)\exp[-2.3(r/300)^2] \quad (7)$$

for $0\leq r\leq 300$ and $0\leq z\leq 600$ m, and $\theta'=0$ elsewhere. The maximum temperature excess θ_0 at cloud center is 3°K in all cases.

At the bounding horizontal surfaces $z=0$ and $z=4.0$ km, we have $w=0$, $\partial u/\partial z=0$, and $\partial v/\partial z=0$. At the radial boundary $r=2.0$ km, we have $u=0$, $\partial w/\partial r=0$, and $v=\Omega\times 2.0$ km. The condition at $r=0$ is $u=0$, $v=0$, and $\partial w/\partial r=0$. The temperature anomaly θ' is constant at $z=0$, $z=4.0$ km, and $r=0$; but $\partial\theta'/\partial r$ vanishes for all time at $r=0$.

Friday (1969) increased the depth of the model from 3 to 4 km to provide a deeper convective layer. He also decreased the grid intervals to 200 m and reduced the time steps to 3 s. Tests showed that further reductions in grid size and time steps would not further reduce the energy losses. The model consists of frictionless axisymmetric motion. A layer deeper than 4 km would have

been desirable, but the Boussinesq approximation of cloud bouyancy becomes less valid as the depth increases. Tests showed profound influence of the upper boundary upon the thermal if the thermal is permitted to contact it, and such effects have thus been avoided by limiting runs to 13 min.

The model was further modified to permit the release of a second thermal into the field of a preceding one at any given time after the release of the first one. Several different time delays between thermals were tried, but the two cases selected for discussion are considered representative for short and relatively long time delays. Even longer time intervals would be desirable but are not practicable for a shallow model.

A two-step Lax-Wendroff (1960) integration method combined with the Gauss-Seidel relaxation formula (National Physical Laboratories 1962) provided the basis for numerical calculations. The computation for a solitary thermal was allowed to run for 13 min, and computer output was obtained at 1-min intervals. The evolution of this thermal was then used as a basis for comparison with "wake affected" thermals. The second-thermal computations proceeded in the same way initially, but then a second thermal having the same initial maximum temperature excess (3°K) was placed into the grid of the first thermal. In case T–3, this was after 2 min. In other words, the grid containing a 2-min-old thermal was used as an initial condition for the second thermal. Comparison is then made between the histories of the two solitary- and combined-thermal events, beginning with the third minute, since no differences appear earlier than this. In case T–8, the second thermal followed the first one after 7 min. The two cases are labeled T–3 and T–8 to associate them with the earliest computer output time in which they may be identified.

Many patterns of isotherms, stream functions, and velocity isotachs were computed and examined for important interaction effects during the course of this study. For economy of illustrations, only a few situations and time frames have been selected to demonstrate the kinds of results that appeared throughout the computations. The patterns have been drawn with the radial scale twice the vertical, to better display features that otherwise would be lost in the crowding of isopleths toward the axis of symmetry, especially in the case of the rotation-influenced thermals.

3. SUCCESSIVE THERMALS WITHOUT ROTATION

Figure 1 shows the evolution of the isotherm patterns for thermals in a nonrotating medium. The evolution of the thermal's shape will be better understood later when the circulation of the thermal is revealed. However, the gradual formation of the "vault" shape of the thermal is due in part to the influx of cooler air at the base pinching in the isotherm pattern and in part to a peripheral downdraft. The vault shape is very pronounced by the 13th minute for both solitary and successive thermals. The vault is also observed in thermals modeled by Ogura (1962).

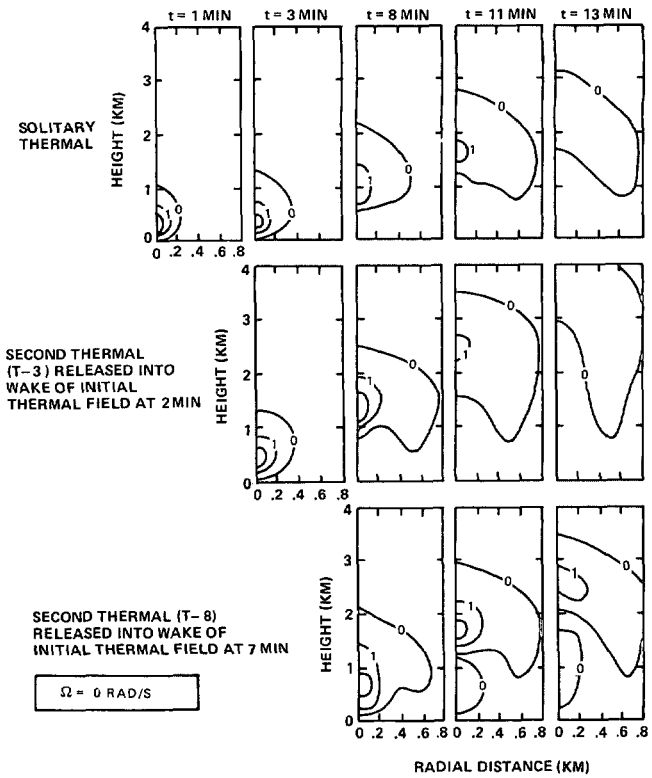

FIGURE 1.—Evolution of isotherm patterns (°K) for solitary and successive thermals without rotation.

The effect of the simulated eddy mixing mentioned earlier may be seen by the rapid merging of the T–3 second thermal with the first one. The T–8 thermal, however, never completely combines with its predecessor during the 13 min that it is observed. The T–3 thermal attains the greatest height after 13 min, but T–8 also rises higher than the solitary thermal. The T–3 thermal, owing to a more vigorous circulation, develops the most pronounced vault.

The height of the maximum temperature zone after 13 min is greatest for T–3, but the rate of rise during the last 6 min is actually greatest for T–8. The reason for this is not known, nor is it clear that T–8 would eventually overtake T–3 if the computer run were extended.

The evolution of the vertical velocities in the thermals is shown in figure 2. The maximum updraft at the center is seen to be enhanced somewhat for the T–3 thermal even at the third minute; and indeed, this is the case throughout its life. The increase in vertical velocity in the ensemble appears to occur almost immediately after release of the T–3 thermal into the field of the first one. This is in part due to the effect of simulated eddy transport of momentum, comparable to the diffusion of heat mentioned earlier. However, note that T–8 does not show any immediate effect from injection of the second thermal. Even after the 13th minute, the vigor of the vertical motion is no greater than that of the solitary thermal, although the center of maximum vertical velocity has risen about 0.3 km higher. Note that downdrafts have formed by this time near the bases of all three thermals. The maximum vertical velocity at the center of the thermal, which is

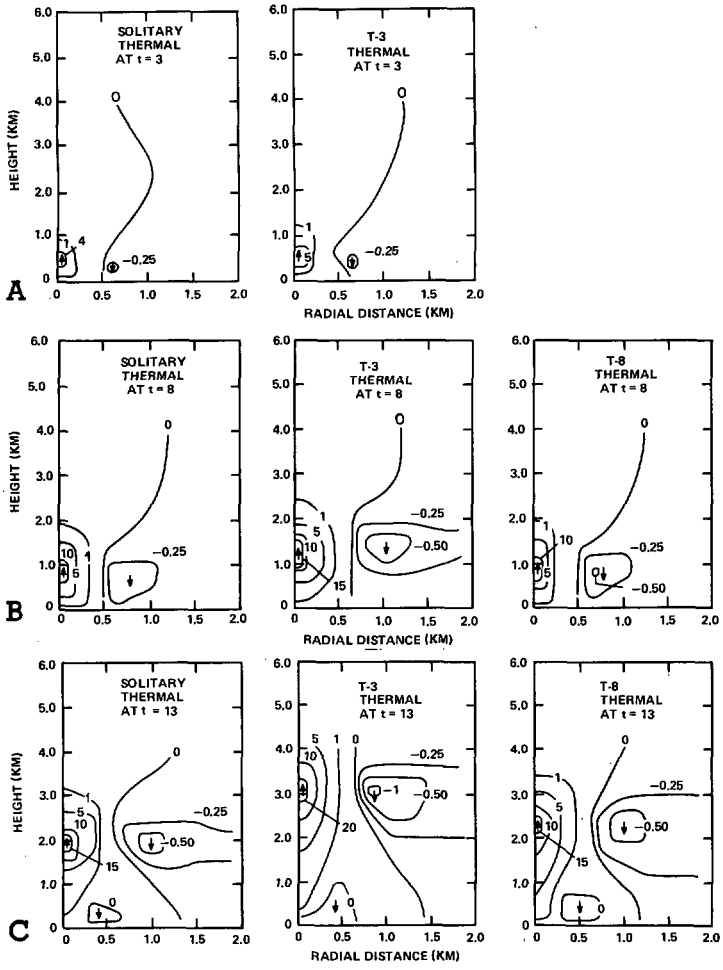

FIGURE 2.—Vertical velocity isotachs (m/s) for solitary and successive thermals without rotation; (A) 3 min after release of initial thermal, (B) 8 min after release of initial thermal, and (C) 13 min after release of initial thermal.

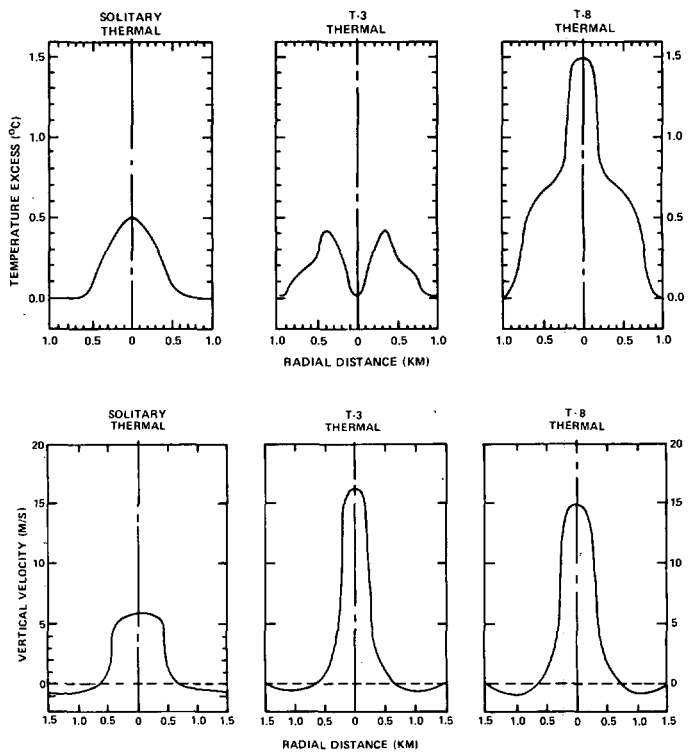

FIGURE 3.—Radial profiles of temperature excess and vertical velocity through thermals at a height of 2.5 km 13 min after release of the first thermal.

about twice the rate of rise in the laboratory experiments, turns out to be about three times the rate of rise of these thermals.

The maximum vertical velocity reaches a peak of 20 m/s in T–3 at 13 min; and the downdraft maximum, which occurs at the same altitude as the maximum updraft, reaches a peak of more than 1.0 m/s. This is the most vigorous vertical motion seen in any of the thermal situations analyzed during this study.

It is natural to inquire whether the patterns of temperature and vertical velocity predicted by the numerical model can provide any special recognition features to distinguish between solitary thermals and interacting successive thermals in the real atmosphere. Figure 3 shows the predicted profiles of temperature excess (over environment) and vertical velocity excess as they would appear on a fly-through by an instrumented aircraft at a height of 2.5 km. The thermals are assumed to be 13 min old, and the speed of penetration is assumed to be great compared with the velocity of rise of the thermal. The most distinctive differences are seen in the temperature profiles, although the increase by a factor of 3 in vertical velocity in the interacting successive thermals might very well stand out in the turbulent responses of the aircraft.

The stream function is a measure of the toroidal circulation intensity in the thermal, and the stream patterns show simultaneously the fields of radial and vertical motion. Figure 4 shows the evolution of the stream patterns for the three types of thermals. The most important features are:

1. The intensity of the circulation increases throughout the period and is stronger for the T–3 thermal. The maximum stream function for T–3 is twice that of the solitary thermal after 13 min, and T–8 is 30 percent greater than the solitary thermal.

2. The radius of the torus increases rapidly to about 0.5 km and remains at that value thereafter, even though the radius of influence of the thermal continues to increase throughout the period. This adherence to a single scale allows the central value of vertical velocity and stream function to increase even while the outer portion of the thermal continues to spread radially. The reason for this tendency for a constant toroid radius is not known. The boundaries of the grid have not been reached; and therefore, the grid cannot have affected the growth of the thermal. The size probably is not a function of the initial buoyancy since T–3 and T–8 also tend toward this size, and these have larger buoyancies than the solitary thermal. Since this model of a thermal has a self-evolving circulation, the tendency toward a characteristic scale must be regarded as a fundamental property. The 13-min period is entirely within the accelerating stage of the thermal; it may be that the radius would begin to increase during the deceleration phase of the thermal.

3. The shape of the circulation pattern changes very little as the thermal grows, and there are no important countercirculations. This part will be more meaningful later when rotation effects are discussed.

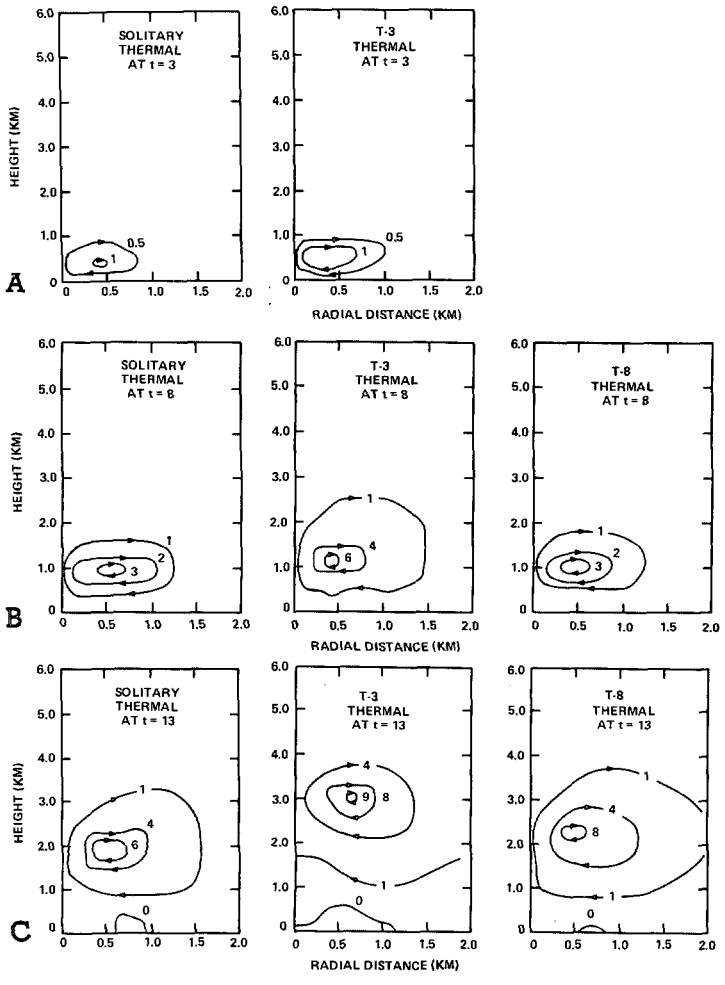

FIGURE 4.—Stream patterns (10^5 m^3/s) for solitary and successive thermals without rotation; (A) 3 min after release of initial thermal, (B) 8 min after release of initial thermal, and (C) 13 min after release of initial thermal.

4. SUCCESSIVE THERMALS IN A ROTATING MEDIUM

Rotation effects are studied by introducing as an initial condition a field of tangential velocity that is zero at the center and increases linearly with radius (the fluid rotates as a solid). Computer outputs have been obtained with other initial vorticities, but the three values used here suffice to illustrate the most important rotation effects. Of course, the initial thermal rearranges the field of tangential velocity so that a subsequent thermal will encounter an initial condition substantially different from that of the first thermal. As we shall see later, a rather pronounced vortex comprises the initial field for the T–8 thermal; and even the T–3 thermal encounters a rotation field typical of a concentrated vortex for the case $\Omega=0.01$ s^{-1}.

TEMPERATURE DISTRIBUTION

Figure 5 gives the evolution of the isotherm patterns for the thermals released into a medium in which the initial

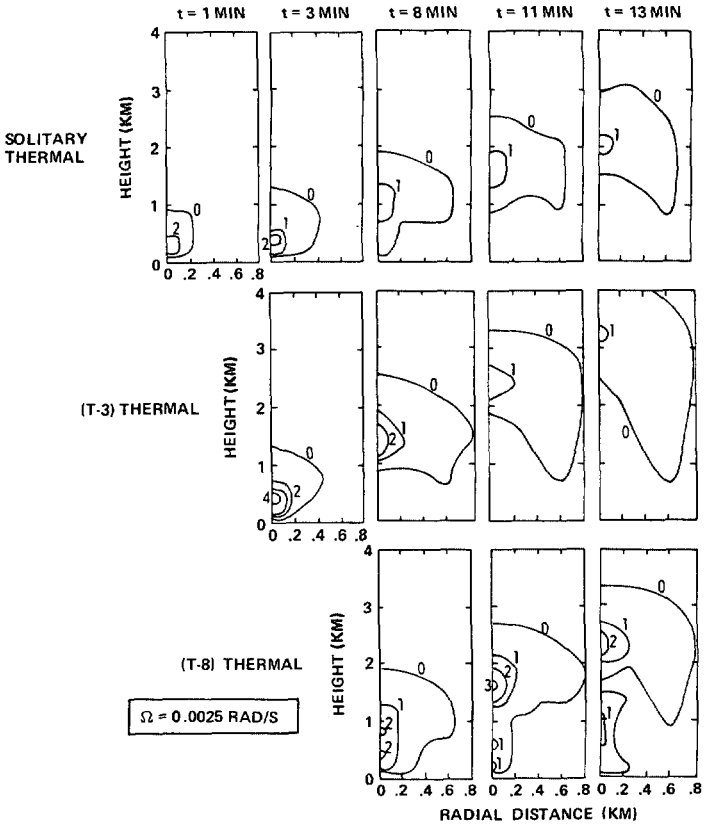

FIGURE 5.—Evolution of isotherm patterns (°K) for rotation-influenced thermals, $\Omega=2.5\times10^{-3}$ s^{-1}.

rotation rate is 2.5×10^{-3} s^{-1}. The effect of rotation can be seen most easily by comparing the three cases with each other as well as with the nonrotation case (fig. 1).

There are some distinct differences in shape for the case 2.5×10^{-3} s^{-1}, and the suppression due to rotation is noticeable, though not pronounced. The rate of heat loss (decrease of central temperature) is less for all three types of thermals, reflecting a smaller mixing rate.

The T–8 thermal still remains separated. The upper portion forms a vault by the 13th minute, and the lower portion is pinched in by cooler air influx to form a "stem."

As the rotation rate is increased, we see from figures 6 and 7 that each of the rotation effects mentioned above becomes even more pronounced. The heat dissipation decreases, the rate of rise of the thermal cap is suppressed, the cylindricity of the cloud shape becomes more pronounced, and the effects of vortex formation are more and more obvious in the shape of the stem. The vault shape becomes less well-defined with increasing rotation rate until it disappears entirely when $\Omega=0.01$ s^{-1}. All of the thermals manage to stretch vertically without actually getting off the ground. This same behavior is observed for rotating thermals simulated in the laboratory. The obvious suppression of volumetric growth of the thermals with increasing Ω was also predicted by theory and observed in quantitative experimental measurements by Wilkins et al. (1971).

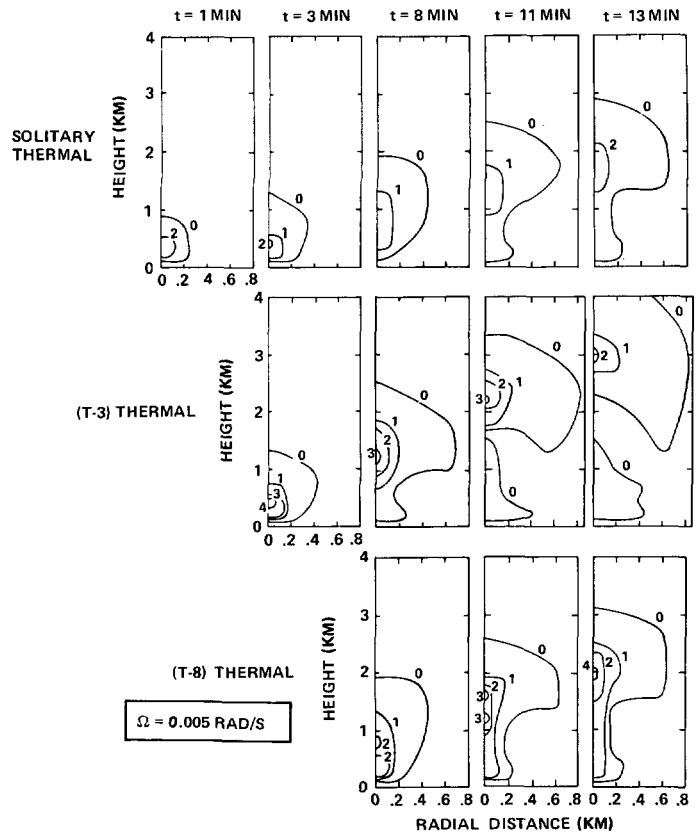

FIGURE 6.—Evolution of isotherm patterns (°K) for rotation-influenced thermals, $\Omega = 5 \times 10^{-3}$ s^{-1}.

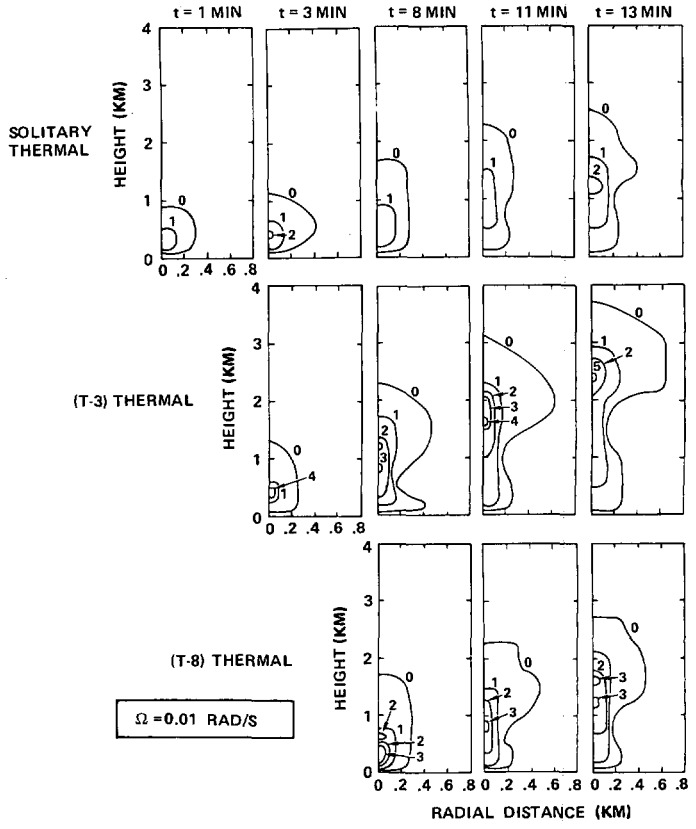

FIGURE 7.—Evolution of isotherm patterns (°K) for rotation-influenced thermals, $\Omega = 10^{-2}$ s^{-1}.

The T–3 thermal shows an odd behavior at $\Omega = 0.005$ s^{-1}. It becomes merged with the initial thermal by the third minute as always but subsequently splits into two thermals as a result of pinching. This is probably due to the greater circulation intensity for T–3, which draws in cooler air despite the tendency for inhibition of the radial velocity component by the rotation field.

The largest rotation rate, which is 0.01 s^{-1} (fig. 7), still shows some pinching but no complete separation of the successive thermals. Apparently, the rotation field is strong enough to inhibit the pinching.

Figures 8 and 9 (and some others later on) are time-history graphs, and their curves have been drawn to originate at height zero for zero time. This is done to aline the curves at the appropriate beginning time; but actually, none of the thermals' features originates at ground level. At time zero, for example, the initial temperature distribution is Gaussian with maximum located 0.3 km above ground. This location is referred to as the "center of lift" of the thermal. The height of the thermal cap is the maximum height attained by the isotherm of zero temperature excess. The zero isotherm was obtained by truncating to zero any temperature excesses falling below 10^{-4} °K.

Figure 8 is a graph of the height of the thermal cap versus time for the two extremes $\Omega = 0$ and $\Omega = 0.01$ s^{-1}. This shows that both of the successive thermals eventually will overtake the preceding one. Note that the suppression is negligible for the more vigorous T–3 thermal, but is quite noticeable for the other two. Another rotation effect is a lengthening of the momentary pause in the rate of rise after the first minute. The pause, though less brief, is also seen for nonrotating thermals. Malkus and Witt (1959) also observed an organization phase in their numerically simulated thermals. This occurs as the turbulent diffusion phase of the thermal, present initially, gives way to domination by the toroidal vortex circulation. When rotation is present in the environment, this lengthening of the pause might be regarded as a rotation-enforced reorganization period in which the thermal rearranges its circulation pattern to better cope with the lateral motion restraints (Taylor-Proudman effect) imposed by the rotation field.

The reorganization period is even more pronounced at the center of lift of the thermal as shown in figure 9 which gives the height of the maximum temperature excess versus time for each of the rotation rates. Even for the zero rotation condition, there is a pause for the solitary and T–3 thermals; and this may be associated with the development of the toroidal circulation, as mentioned earlier. The largest rotation rate gives the longest pause; and for this case, even the T–8 thermal exhibits a reorganization period which is not evident for any of the lesser rotation rates. The solitary thermal,

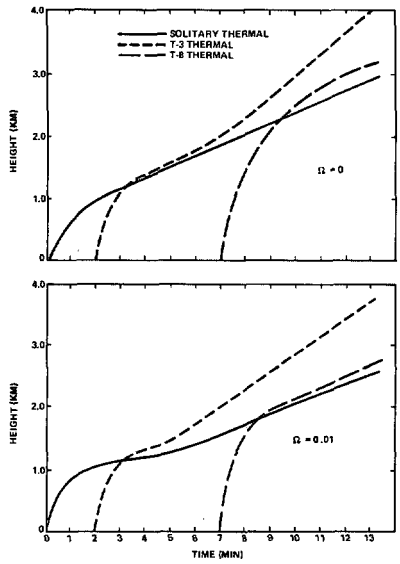

FIGURE 8.—Height of rise of the thermal cap versus time for thermals with and without rotation in the environment.

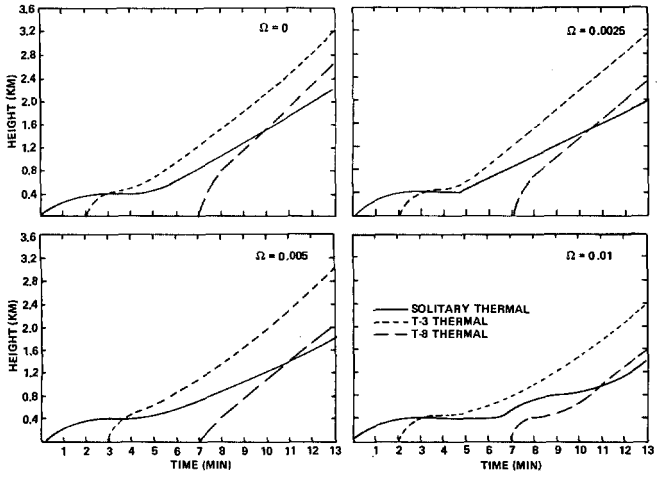

FIGURE 9.—Height of maximum temperature excess versus time for four different rotation rates in the environment of the thermals.

which is the oldest of the three, shows two separate pauses in the rate of rise; and this suggests an oscillatory motion. An oscillatory effect will also be seen later in the magnitude of the maximum tangential velocity excess.

It is interesting to note in comparing figures 8 and 9 that, for $\Omega=0$, the vertical distance between the solitary thermal's center of lift and its thermal cap increases rapidly to 600 m by the third minute but increases very little thereafter. However, for $\Omega=0.01$ s^{-1}, this spacing is 720 m by the third minute and increases to 1360 m by the 13th minute. This is due to the extreme rotational suppression of the zone of maximum temperature and also testifies to the pronounced vertical stretching of the thermal. This suppression occurs despite the fact that the rate of heat loss is markedly less for rotation. Thus we have the paradox, true for all three thermals, that extreme suppression occurs for the center of lift despite the increased

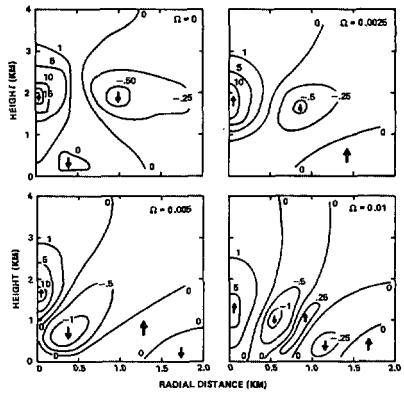

FIGURE 10.—Rotation effects on the solitary thermal's pattern of vertical velocity isotachs (m/s) shown at age 13 min.

concentration of buoyancy there. Although this feature does not disagree especially with our intuitive notion of what should occur, it is not very likely that the existence of this feature would be realized without a numerical simulation of some kind.

VERTICAL VELOCITY DISTRIBUTIONS

Figures 10 through 12 show the patterns of vertical velocity that evolve by the 13th minute for each of the three types of thermals and for each of the four initial rotation rates. These patterns reflect the effects of rotation even more than do the isotherm patterns.

The vertical velocities for all three thermals are distributed as normally expected for toroidally circulating buoyant clouds when $\Omega=0$. The first effect of rotation is a downward tilt of the outer portion of the toroid (i.e., the outer portion is suppressed relatively more than the the central portion). The second effect is the generation of countercirculations. There are three reversals in the direction of vertical velocity for $\Omega=0.005$ s^{-1} (proceeding radially outward from the central updraft) and four reversals for $\Omega=0.01$ s^{-1}. The alternating updrafts and downdrafts definitely are a feature of strong interaction between the thermal and the rotation field, and this feature evidently is a manifestation of the "Taylor columns" which are sometimes seen in laboratory experiments with rotating fluids. The suppression of the peripheral downdraft reaches the extreme for the T–3 thermal since the zone of maximum downdraft appears almost directly beneath the updraft.

The magnitudes of the vertical velocities are reduced by rotation for all but the T–8 thermal which actually shows a velocity enhancement for $\Omega=0.0025$ s^{-1}. This turns out to be the only case of rotational enhancement of any velocity (other than tangential) that has been discovered during this investigation.

Downdraft velocities that develop for the rotational situations are in all cases considerably larger than for nonrotational situations.

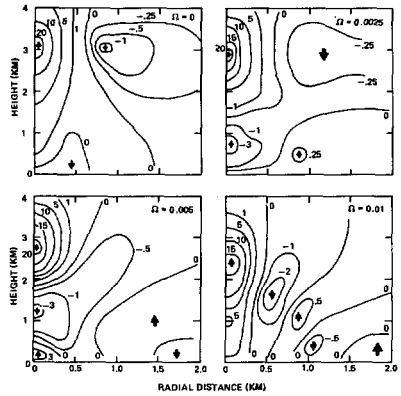

FIGURE 11.—Rotation effects on the T-3 thermal's pattern of vertical velocity isotachs (m/s) shown 13 min after release of the initial thermal.

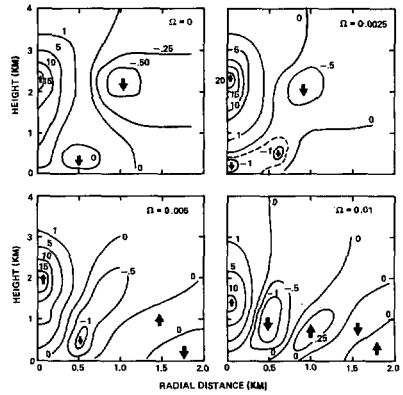

FIGURE 12.—Rotation effects on the T-8 thermal's pattern of vertical velocity isotachs (m/s) shown 13 min after release of the initial thermal.

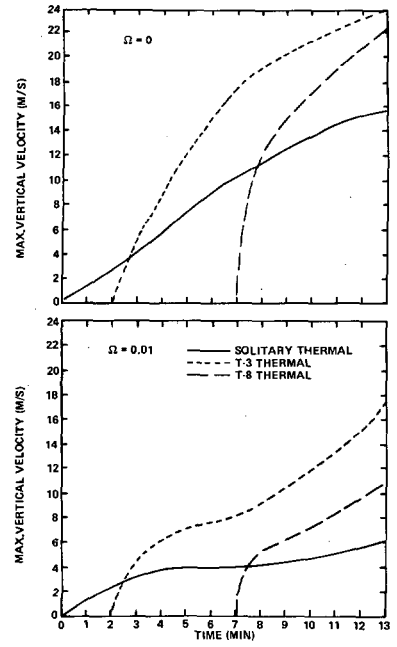

FIGURE 13.—Maximum vertical velocity versus time for thermals with and without rotation influence.

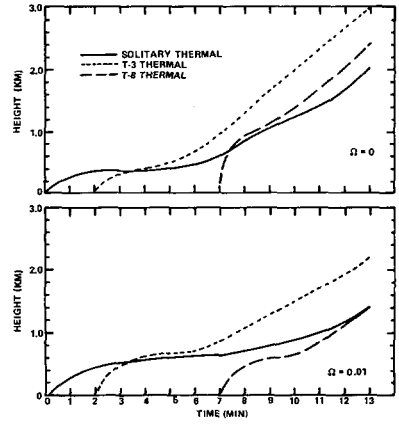

FIGURE 14.—Height of maximum vertical velocity versus time for thermals with and without rotation influence.

Figure 13 shows very graphically the suppression of the maximum vertical velocity that occurs for the largest of the rotation rates. The solitary thermal is the one most suppressed, for its maximum updraft remains practically constant after the fourth minute. Figure 14 gives the height of the maximum updraft versus time; and comparison with figure 13 shows that, while the vertical velocity of the T-8 thermal surpasses that of the solitary thermal almost immediately when $\Omega=0.01$ s^{-1}, its height above ground does not catch up with the solitary thermal until the 13th minute. The height of maximum vertical velocity corresponds very closely, minute by minute, to the height of the maximum temperature excess for all three thermals, and this feature is unaffected by rotation.

STREAM PATTERNS

The stream-function distributions, which are displayed in figures 15 through 17 on the same format as were the vertical velocity isotachs, are a measure of the intensity of the toroidal circulation. There are no surprises in light of what was revealed previously. The rotation effects are:

1. Suppression of vertical growth and stream-function magnitudes;
2. Vertical elongation of the main cell;
3. Evolution of countercirculations radially, with four separate and distinct cells for the strongest interaction, $\Omega=0.01$ s^{-1}.

It is interesting to note that the thermal simulated by Ogura (1963), while not concerned at all with rotation, also exhibits the alternating cells of countercirculation. The clue as to why this does not occur for the nonrotation cases computed here lies in the fact that these thermals (except for T-3) were not permitted to contact the upper boundary of the grid, in contrast to Ogura's thermal (our grid is 1 km deeper than Ogura's). This implies that partitioning of energy into countercirculation cells occurs as a result of suppression of the vertical motion, whether by a rotation field or by a "lid."

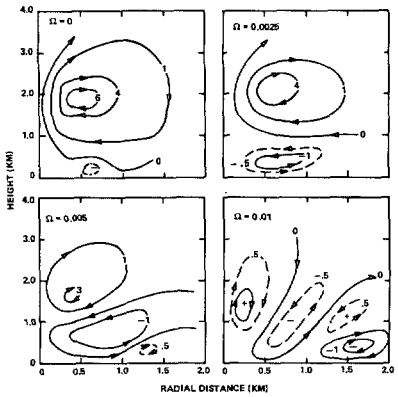

FIGURE 15.—Rotation effects on the solitary thermal's stream pattern (units, 10^5 m^3/s) shown at age 13 min.

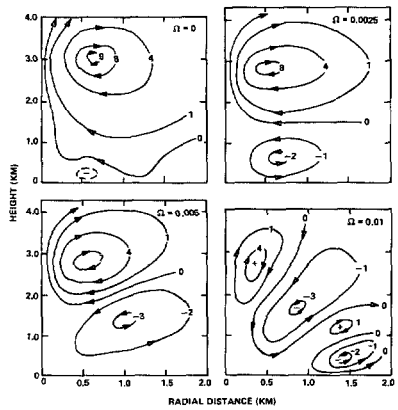

FIGURE 16.—Rotation effects on the T-3 thermal's stream pattern (units, 10^5 m^3/s) shown 13 min after release of the initial thermal.

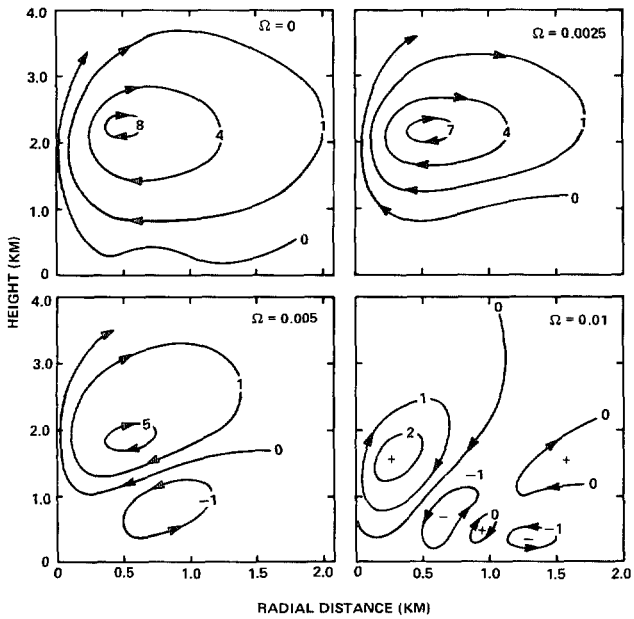

FIGURE 17.—Rotation effects on the T-8 thermal's stream pattern (units, 10^5 m^3/s) shown 13 min after release of the initial thermal.

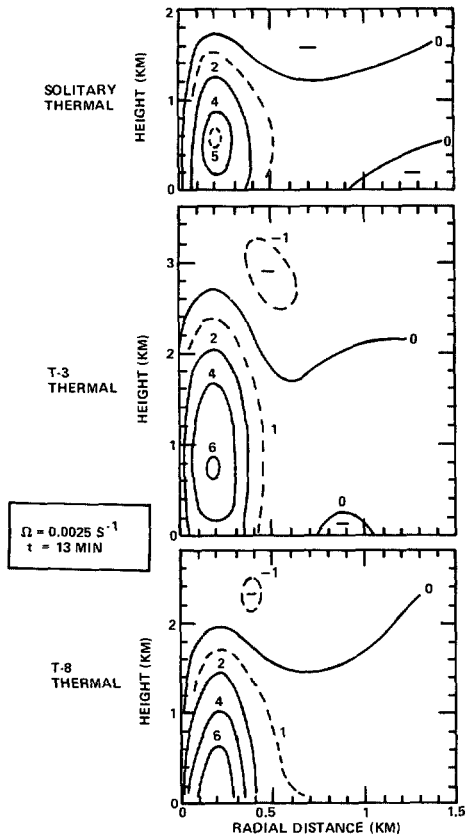

FIGURE 18.—Tangential velocity isotachs (m/s) for vortexes formed by solitary and successive thermals at age 13 min; environmental rotation rate $\Omega = 0.0025$ s^{-1}.

5. VORTEX FORMATION

For visualization of changes in the tangential velocity field brought about by the solitary and successive thermals, it is necessary to keep in mind that the starting condition is one in which the radial profile is linear (solid rotation). The radius versus height pattern of the tangential velocity isotachs would appear initially as a field of vertical parallel lines. For example, for $\Omega = 0.0025$ s^{-1}, the 2.5 m/s isotach would be located initially at a distance of 1 km from the axis of symmetry. Such a weak rotation field would never be detected in a conventional synoptic network.

The fields of tangential velocity shown in figures 18 through 20 represent only the increases in velocity brought about by the interaction of the thermals with the initially rather weak tangential velocity field. The much stronger velocity field that evolves by the 13th minute is indicative of the amount of kinetic energy that was removed from the thermal during vortex formation and transposed into the tangential velocity field. This accounts for the observed suppression; since the suppression increases with rotation rate, we should expect that the vortex intensity should increase also. This is true up to a point. A notable exception here is the solitary thermal that actually forms the least intense vortex for the

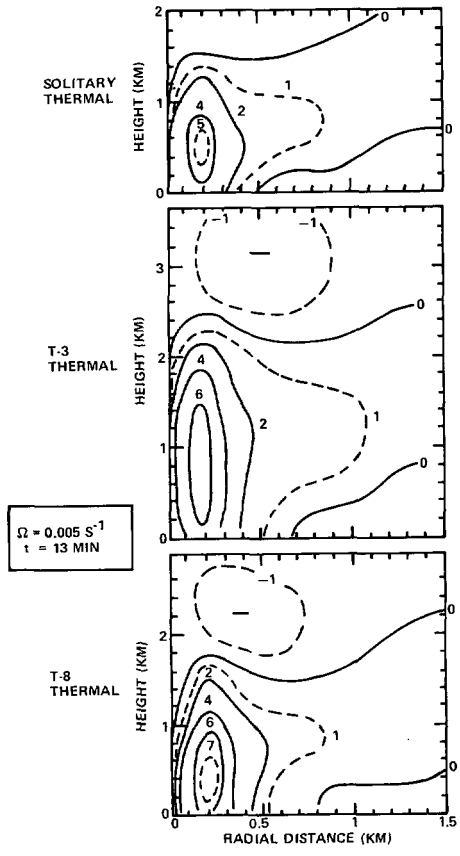

FIGURE 19.—Same as figure 18, except $\Omega=0.005\ s^{-1}$.

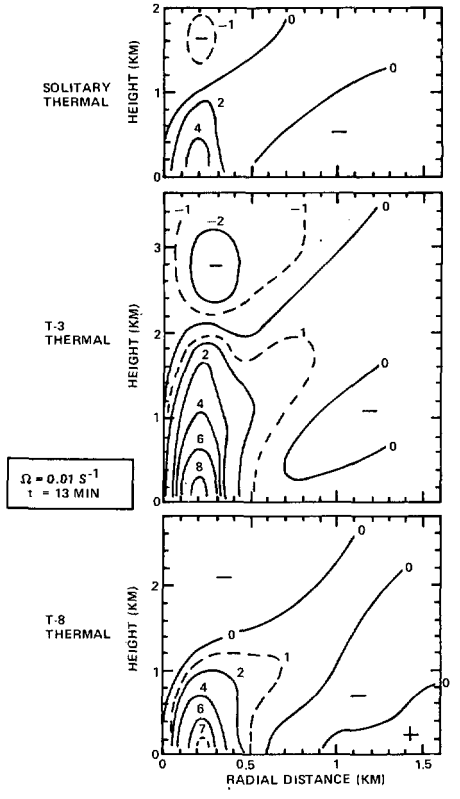

FIGURE 20.—Same as figure 18, except $\Omega=0.01\ s^{-1}$.

largest of the initial rotation rates. This is obviously the result of insufficient buoyancy in the solitary thermal. We say that a buoyant cloud is "rotation dominated" whenever increasing the initial rotation rate results in the formation of a weaker vortex rather than a stronger one. This suggests that there are optimum combinations of cloud buoyancy and ambient vorticity that give the strongest interactions. This effect might be viewed as a purely geometric consideration in the case of the solitary thermal; since the center of the toroidal circulation only rises to 1.3 km, the vortex formation region, which necessarily is below the torus, may be too restricted in depth to allow the most efficient interaction to proceed. The T–8 thermal appears to have been similarly affected, but to a lesser extent.

We note also that the zone of maximum vortex intensity remains at ground level for $\Omega=0.01\ s^{-1}$. However, even though the maximum intensity zone rises above ground for the other rotation rates, this does not imply that the vortex itself breaks contact with the ground.

Anticyclonic countercirculation occurs above the vortex in all cases but attains its greatest intensity above the T–3 thermal at $\Omega=0.01\ s^{-1}$. These countercirculations coincide with the regions of divergence as they appear on the stream patterns, as might be expected.

Since the suppression of the thermal increases with rotation rate, it is not surprising that the height attained by the vortex is also suppressed by increased rotation rate. If we define the height of the vortex in terms of the zero tangential velocity isotach, then we see that the heights attained within 13 min are as shown in table 1. The heights attained by the thermal caps are included for comparison.

The height of the vortex formed by the solitary thermal is reduced by one-half between $\Omega=0.0025\ s^{-1}$ and $\Omega=0.01\ s^{-1}$, whereas the height of the thermal cap is reduced by only one part in six. The suppression is also proportionately greater for the vortex formed by the other thermals. This is a further manifestation of the vertical stretching effect noted earlier in the suppression of the center of lift. *The vertical spacing between the thermal cap and any circulation feature below the cap increases with rotation rate.* We note also that this vertical elongation of the cloud features could give the impression that the system is a continuous plume rather than a discrete thermal or an ensemble of discrete thermals.

TABLE 1.—*Heights attained in 13 min (km)*

Thermal	Thermal cap				Vortex		
	Ω=0.0	0.0025	0.005	0.10 s^{-1}	Ω=0.0025	0.005	0.10 s^{-1}
Solitary	3.1	3.0	2.9	2.5	1.7	1.5	0.9
T-3	>4.0	>4.0	>4.0	3.7	2.7	2.4	2.1
T-8	3.5	3.3	3.1	2.7	2.0	1.8	1.3

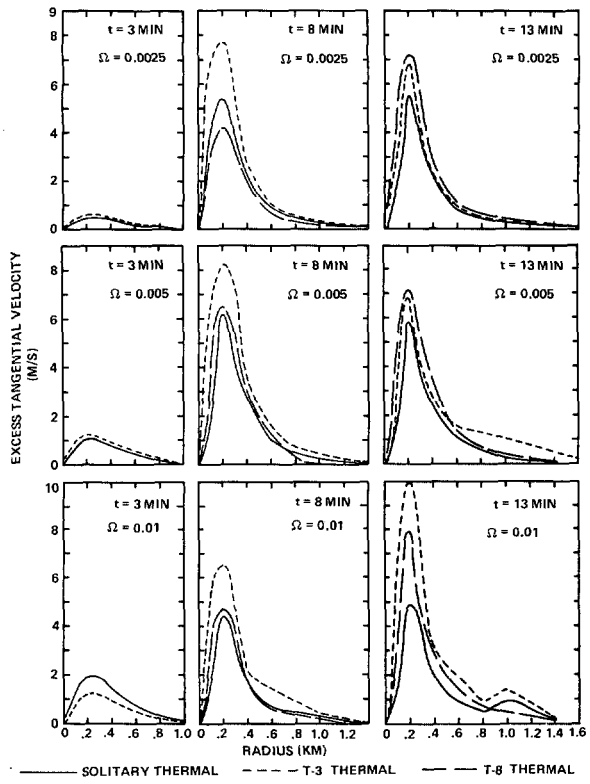

FIGURE 21.—Radial profiles of tangential velocity for vortexes generated by successive thermals shown at 3, 8, and 13 min. The profiles are made through the location of maximum tangential velocity in each case.

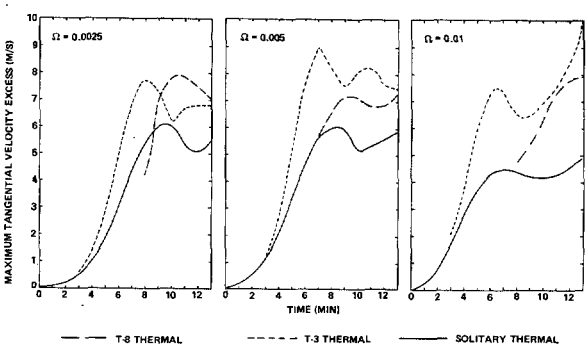

FIGURE 22.—Maximum tangential velocity versus time for vortexes formed by solitary and successive thermals.

Another feature that becomes more pronounced with rotation rate is the branching radially outward and upward of the tangential velocity isotachs to give a funnel shape to the pattern. For $\Omega=0.01$ s^{-1}, the pattern evolves into one that accords with the alternating sign of circulation noted in the stream functions and the vertical velocity isotachs. It should be recalled that these patterns are plotted with the radial scale twice the vertical scale; thus the slopes of these elongated cells are actually steeper than they appear in these illustrations.

The radial profiles of tangential velocity are shown in figure 21. The profiles are characterized by a maximum at a radius of 200 m and a shape that is approximately "irrotational" beyond 220 m. Figures 18–20 show that the radius of maximum velocity does not vary with height, and figure 21 shows that the radius also does not vary with time, rotation rate, or type of thermal. This remarkable adherence to a prescribed scale is even more surprising in view of the fact that the amount of buoyancy is so different for the different thermals. The scale of the vortex is evident by the third minute. The boundaries of the grid could not have been reached by any part of the cloud this early; and therefore, grid dimensions seem not to be indicated as the cause for the scaling effect. There is nothing in the appearance of the isotherms, stream functions, or vertical velocity isotachs to suggest that this scale effect should be present, although, as noted earlier, the radius of the toroidal circulation of the thermal rapidly increases to 0.5 km and remains at that value thereafter. Thus, it appears that whatever is responsible for setting the scale of the torus also determines the scale of the vortex.

The T–3 thermal achieves a vortex intensity of 10 m/s for $\Omega=0.01$ s^{-1} by the 13th minute. This is the greatest intensity of any of the profiles in figure 21, and figure 22 shows that the maximum velocity (or sleeve velocity) is still increasing sharply at this time. The vertical velocity was also seen to be increasing sharply at the 13th minute, and the heat loss (and hence the buoyancy loss) was very small (temperature excess at the center of lift was still 5°K). In view of this, it seems reasonable to expect that the T–3 ensemble of thermals might easily reach a vortex intensity of 25–30 m/s if the computation could be continued.

The oscillatory behavior is more pronounced in the sleeve velocity than in any of the other variables plotted against time, although figure 9 did show an oscillation for the height of rise of the maximum temperature region of the solitary thermal whenever $\Omega=0.01$ s^{-1}. The pause or reorganization period is likely associated with the first oscillation in the series. We see now, comparing figure 22 with figure 9 for example, that the pause in the rate of rise coincides with the sharpest rate of increase in vortex intensity. In other words, the pause in vertical motion occurs when the kinetic energy of the thermal is being utilized for vortex formation. Once the vortex is formed, the thermal recovers and continues upward until the restraint imposed by the rotation field again dominates the motion field, causing still another "reorganization" period.

The magnitude of the first peak in vortex intensity and its time of occurrence are shown in table 2. This shows that there is a tendency for the peak to occur earlier as the rotation rate increases. For a solitary thermal, there is also a tendency for the magnitude of the first peak to be smaller as the rotation rate increases; but this trend is not evident for successive thermals.

TABLE 2.—*Time and magnitude of the first peak in vortex intensity for solitary, T-3, and T-8 thermals as a function of rotation rate*

Thermal	Time			Magnitude		
	Ω=0.0025	0.005	0.01 s^{-1}	Ω=0.0025	0.005	0.01 s^{-1}
Solitary	9.5	8.4	7.0 min	6.0	6.0	4.2 m/s
T-3	7.3	7.0	6.5 min	7.6	9.0	7.4 m/s
T-8	10.6	9.5	~13.0 min	7.9	7.1	~8.0 m/s

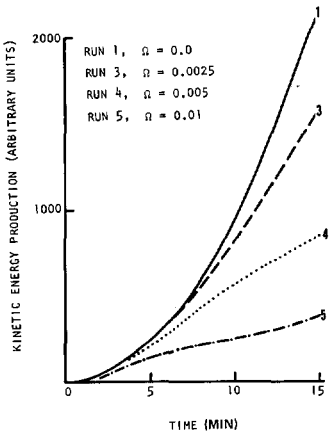

FIGURE 23.—Potential to kinetic energy conversion for solitary thermals.

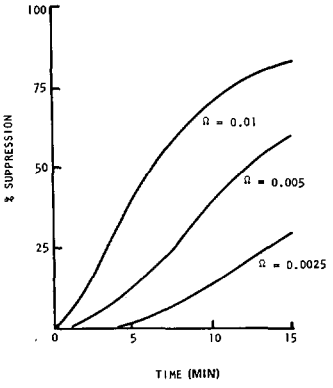

FIGURE 24.—Suppression of kinetic energy production as a function of rotation.

6. ENERGY CONSERVATION AND TRANSITION

Studies of the energy budgets for solitary thermals on this project were made by Friday (1969). Only a small fraction of the available potential energy is converted during a 15-min computer run; and hence the losses incurred, between 5 and 10 percent in all cases, were essentially potential energy.

Figures 23–26 summarize the energy transitions for four different rotation rates. The rate of conversion to total kinetic energy is shown in figure 23. The only

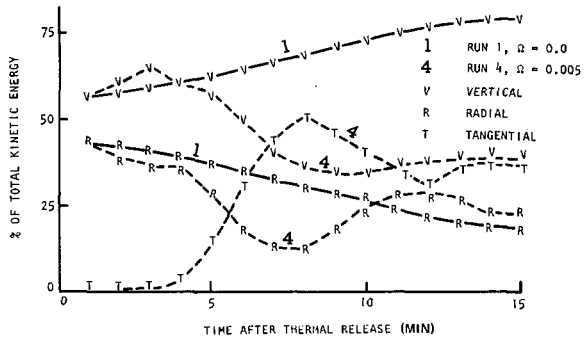

FIGURE 25.—Energy budget for runs 1 and 4 (breakdown of total kinetic energy into vertical, radial, and tangential components).

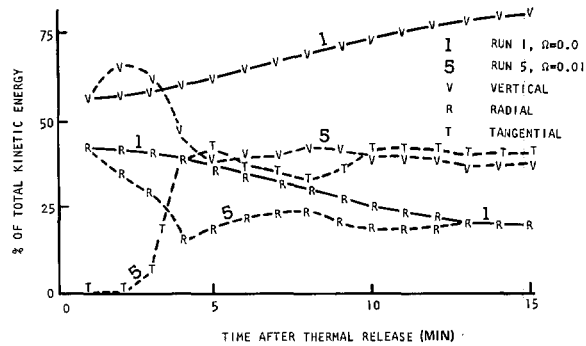

FIGURE 26.—Energy budget for runs 1 and 5 (breakdown of total kinetic energy into vertical, radial, and tangential components).

variable parameter among the four runs is the initial angular velocity of the environmental fluid. Thus, we conclude that the rate at which the potential energy of a buoyant mass is converted to the kinetic energy of motion is suppressed as the rotation rate increases. A graphical illustration of the exact degree of suppression is given in figure 24 that shows the amount of suppression of conversion rate as a function of the initial angular velocity of the environmental fluid. The curves give percentage suppression of kinetic energy relative to a thermal in a nonrotating fluid. The percentage suppression clearly increases with rotation rate. The thermal for Ω=0.01 rad/s is 82 percent suppressed after 15 min.

Detailed energy budget studies have been made for three of the four adiabatic runs illustrated in figure 23. In these, the total kinetic energy at each minute of the numerical computation was divided into three different portions. These consisted of the kinetic energy due to vertical velocities, radial velocities, and, in the case of the rotation studies, the tangential velocities. In the rotating-environment situations, the initial kinetic energy of the rotation field was subtracted from the final results; therefore, the curves labeled "T" represent excesses over the initial kinetic energy rather than absolute values. These three fractions were then plotted in terms of the percentage of the total integrated kinetic energy within the numerical grid and are depicted in figures 25 and 26.

The results for nonrotation cases are illustrated by the solid lines in figures 25 and 26. These have been repeated in both figures for ease in comparison. One minute after thermal release, the vertical velocity accounts for 57 percent of the kinetic energy; and the remaining 43 percent is due to the radial velocities. As the thermal continues to grow, that portion of the kinetic energy due to the vertical velocity increases smoothly and monotonically until it amounts to 80 percent of the total at the end of 15 min.

A remarkable contrast is shown in run 4 where the rotation speed is 0.005 rad/s. At 1 min after thermal release, the distribution is the same as for the nonrotation case; the rotational energy is still negligible. Although the percentage of kinetic energy present in the tangential velocity is essentially negligible for the first 3 or 4 min, the rotational field has a marked effect on the amount of energy distributed between the vertical and radial velocity components. At 2 and 3 min after thermal release, the vertical velocity is seen to account for a greater percentage of the kinetic energy than it did in the nonrotating case. This can be attributed to the suppression of the radial motion by the rotational field. By 5 min after release, the percentage of kinetic energy contained in the tangential field is seen to be increasing at a rapid rate. This increase is at the expense of both the vertical and radial components. The vertical component lags a little behind the radial component in the decrease shown after 5 min, but the general shape of the two curves is similar. These two curves are out of phase with the tangential component. After the maximum is reached by the tangential component, it begins to drop, allowing the share of the kinetic energy contained in the vertical and radial velocity components to increase slightly. The last 5 min of the thermal growth gives the general impression of a damped oscillatory motion, with the radial component of kinetic energy approaching the same share of the kinetic energy as it had for the nonrotating case. The percentages of kinetic energy contained in the vertical and tangential components appear to approach each other. After 15 min, therefore, the energy contained in the radial component is approximately the same as in the nonrotating case. The energy contained in the nonrotating thermal's vertical component appears to become equally divided between the vertical and tangential components whenever a vortex-forming interaction occurs.

Figure 26 presents the energy budget for $\Omega=0.01$ rad/s. At this higher rotation rate, the characteristics that were noted in figure 25 become even more apparent. Initially, the vertical and radial components are the same with or without rotation. At 2 and 3 min after release, the kinetic energy of the vertical component is greater as a result of rotation. The tangential component begins to become important at an earlier time for this higher rotation rate, and a strong increase is apparent at 3 and 4 min after thermal release. The tangential component has reached a maximum after 5 min and then begins a damped oscillatory motion. This maximum occurs at an earlier time than for the smaller rotation rate, but the value of the maximum is actually smaller. This result is consistent with those for the maximum tangential velocity excess, as shown in figure 22.

7. CONCLUSIONS

The subject of successive thermal interactions is most complex, especially when vortex formation is included in the analysis. The numerically simulated self-evolving thermal of the Ogura type is shown to be a valuable analytical tool for the study of the complex interactions that occur as the thermals interact with the rotation field and with each other. Some realism is lost because of the limitations imposed by the several simplifying assumptions, but probably the most serious limitation lies in the restriction to a shallow layer. All of the thermals analyzed here are very young, since none had entered the decelerating stage. It is important to learn the nature of the interactions during the decelerating stage as well. The realism of the simulation can be improved easily with the addition of eddy viscosity and the nonadiabatic effects of cloud buoyancy increasing with time, but the main features of the interactions are displayed just as well without these additions.

The realism of the simulation must suffer somewhat from the neglect of surface friction in those situations involving rotation. This is especially true for the largest rotation rate, $\Omega=0.01$ s^{-1}, since the vortexes formed keep their tangential velocity maxima in contact with the ground, as seen in figure 20. On the other hand, figures 15–17 show that the maximum circulation intensities break contact with the ground and rise with the thermals, regardless of rotation rate. If surface friction had been included in the model, we would expect the tangential velocities near the ground to be reduced also. A friction-induced radial inflow component would then add to the vertical velocity at the center of the thermal and possibly also would increase the rate of rise of the thermal cap. It is conceivable that this effect, combined with the reduction in heat loss, could actually give a net rotational enhancement in the rate of rise of some thermals. However, surface friction was present for the rotating thermal tank experiments of Wilkins et al. (1971), and these experiments showed the suppression to increase with rotation rate. The question will not be easily resolved for the real atmosphere, but some idea of the importance of the surface friction effect might be obtained by adding a boundary layer to the present model. This additional investigation seems well justified; but since it will involve extensive redesign of the model and many computer runs to evaluate the effects of the Ekman layer parameters, the task is beyond the scope of this paper.

Even though the initial thermal had not reached the deceleration stage, the second one was still able to overtake it very quickly, even the T–8 thermal. Of course,

after the overtaking, all observations are referred to the ensemble, since there is no way to identify the thermals separately. The successive thermals simulated in the laboratory by Wilkins et al. (1971) were in the deceleration stage before overtaking occurred, so the two experiments differ somewhat in this respect. Also, all observations and theoretical predictions were referred to the second thermal, rather than to the ensemble. Nevertheless, there are some areas of basic agreement between the two. These are:

1. Enhancement in rate of rise of the second thermal owing to the wake effect from the first thermal;
2. Overtaking of the first thermal by the second one, provided that the time delay between thermals is not too long;
3. Suggestion that some optimum combination of cloud buoyancy and ambient vorticity will result in the formation of the most intense vortex;
4. Increased suppression of the rate of rise of the thermal cap as the rotation rate increases;
5. Change of cloud shape from spheroidal to cylindrical, combined with increased inhibition in the cloud's volumetric growth rate, as the rotation rate is increased;
6. Formation of "Taylor columns" when there is a sufficiently strong interaction between the thermal and the rotation field; and
7. Excessive suppression when the buoyancy of the cloud is small compared to the ambient vorticity; the thermal becomes rotation dominated and generates neither a strong vortex nor a vigorous toroidal circulation.

Attempts were also made in the laboratory to simulate successive thermals in a rotating medium, but these attempts failed due to the tendency for rotation to keep the first thermal in contact with the bottom of the thermal tank, thereby obscuring the second thermal. A technique is now in development in which the preceding thermal can be made transparent; and hopefully, this may overcome the experimental difficulty.

When the first thermal forms a concentrated vortex, the ambient vorticity field is entirely changed for subsequent thermals; and this should be reflected in their behavior. Of course, the T–8 thermal encounters the most concentrated vortex as was shown by figure 21. We recall that the anomaly associated with this thermal is an absolutely unique enhancement in its vertical velocity for $\Omega=0.0025\ s^{-1}$. Figures 21 and 22 show that T–8 also achieves the most intense vortex for this rotation rate. The suggestion is clear that the preceding thermal carried out most of the chore of vortex formation, leaving T–8 to proceed with less encumbrance from the rotation field. Thus $\Omega=0.0025\ s^{-1}$ must be very nearly optimum for the T–8 thermal; the inhibition of lateral mixing keeps the buoyancy force sufficiently concentrated to more than compensate for the loss of the thermal's kinetic energy to the field of tangential velocity. The theory derived by Wilkins et al. (1971) also provides for rotational enhancement in the rate of rise of the thermal caps; but unfortunately, the theory contains a parameter that can be evaluated only crudely from inferences based on the observed behavior of the thermals themselves.

We observe a strong tendency for the toroidal circulation to grow rapidly to a radius of 500 m and to remain at that size regardless of circumstances. Due to this tendency, the vortex that forms whenever rotation is present grows rapidly to a radius of 200 m and adheres to that size thereafter. Because of the shallow convection model, we have investigated only the early part of the lives of the thermals or the predeceleration stage. It would be interesting to learn whether this "scaling" effect also occurs at a later stage.

A discrete thermal element may under rotation influence take on some of the features of a steady plume. This is the result of the vertical elongation. The impression of a steady-state situation may also result from the tendency for any vortex formed to remain at a constant size. Also, the boundaries between two or more successive thermals may be obscured due to the rotation inhibition of the pinching inward of cooler air to form the characteristic stem.

There is not general agreement that atmospheric vortexes such as tornadoes and dust devils can be generated by isolated buoyant elements or even by a series of such elements, although there is nothing in the results of the laboratory and numerical simulations to suggest that solitary and successive thermals cannot form intense vortexes. It is hoped that those who are opposed to this concept of vortex generation by thermals will still be interested in the interactions between successive thermals in a nonrotating medium. The assumptions used in the development of this numerical model make it appear to be more applicable to dust devil formation than to tornadoes; however, it was found that the main features of the vortex formation interaction are essentially the same whether the thermal is "dry" or has buoyancy increasing with time. We conclude that at least some of the results must also be applicable to tornado formation. Once a tornado is formed, its sink may be maintained by successive buoyant elements or a plume entering laterally at some height above the vortex. On the other hand, a vortex may have a lifetime of several minutes without ever entering into this steady-state condition.

ACKNOWLEDGMENTS

This research is supported by the Atmospheric Sciences Section of the National Science Foundation under Grant GA–16350. The authors are also grateful to Drs. R. L. Inman and E. W. Friday, Jr., and to Maj. R. Rinaldi, U.S. Air Force, whose earlier numerical simulations of rotation-influenced convection as part of this project provided us with much of the experience required for proceeding with the study of successive thermals and vortex formation.

REFERENCES

Chandrasekhar, Subrahmanyan, "The Instability of a Layer of Fluid Heated From Below and Subject to Coriolis Forces," *Proceedings of the Royal Society of London*, Ser. A, Vol. 217, No. 1130, England, May 7, **1953**, pp. 306–327.

Chandrasekhar, Subrahmanyan, *Hydrodynamic and Hydromagnetic Stability*, Clarendon Press, Oxford, England, **1961**, 652 pp. (see pp. 83–85).

Dropkin, David, and Globe, Samuel, "Effect of Spin on Natural Convection in Mercury Heated From Below," *Journal of Applied Physics*, Vol. 30, No. 1, Jan. **1959**, pp. 84–89.

Friday, Elbert W., Jr., "Behavior of Discrete Convective Elements in a Rotating Fluid," *Final Report* ARL–1649–1, Contract No. NSF–GA–1328, University of Oklahoma, Norman, May **1969**, 134 pp.

Fujita, Tetsuya T., Wilk, Kenneth E., and Fankhauser, James C., "A Proposed Explanation of Deviate Paths of Echo Couplets," *Proceedings of the Twelfth Conference on Radar Meteorology, Norman, Oklahoma, October 17–20, 1966*, American Meteorological Society, Boston, Mass., Oct. **1966**, pp. 347–355.

Fultz, Dave, and Nakagawa, Yoshinari, "Experiments on Over-Stable Thermal Convection in Mercury," *Proceedings of the Royal Society of London*, Ser. A, Vol. 231, No. 1185, England, Aug. 22, **1955**, pp. 211–225.

Giles, James D., "An Investigation of the Mesoscale Pattern Associated With Severe Storms," M.S. thesis, University of Oklahoma, Norman, May **1967**, 40 pp.

Goroff, I. R., "An Experiment on Heat Transfer by Over-Stable and Ordinary Convection," *Proceedings of the Royal Society of London*, Ser. A, Vol. 254, No. 1279, England, Mar. 8, **1960**, pp. 537–541.

Inman, Rex L., "The Evolution of Convective Motions in a Rotating Fluid," Ph. D. thesis, Texas A&M University, College Station, May **1966**, 90 pp.

Kuo, Hsiao-Lan, "On the Dynamics of Convective Atmospheric Vortices," *Journal of the Atmospheric Sciences*, Vol. 23, No. 1, Jan. **1966**, pp. 25–42.

Lax, Peter D., and Wendroff, Burton, "Systems of Conservation Laws," *Communications on Pure and Applied Mathematics*, Vol. 13, Interscience Publications, Inc., New York, N.Y., **1960**, pp. 217–237.

Lilly, Douglas K., "On the Numerical Simulation of Buoyant Convection," *Tellus*, Vol. 14, No. 1, Stockholm, Sweden, May **1962**, pp. 148–172.

Lilly, Douglas K., "Numerical Solutions for the Shape-Preserving Two-Dimensional Thermal Convection Element," *Journal of the Atmospheric Sciences*, Vol. 21, No. 1, Jan. **1964**, pp. 83–98.

Lilly, Douglas K., "Experimental Generation of Convectively Driven Vortices," *Geofisica Internacional*, Vol. 5, No. 2, Mexico City, D. F., Mexico, Apr. **1965**, pp. 43–48.

Long, Robert R., "Sources and Sinks at the Axis of a Rotating Liquid," *Quarterly Journal of Mechanics and Applied Mathematics*, Vol. 9, No. 4, Oxford University Press, London, England, Dec. **1956**, pp. 385–393.

Long, Robert R., "Vortex Motion in a Viscous Fluid," *Journal of Meteorology*, Vol. 15, No. 1, Feb. **1958**, pp. 108–112.

Long, Robert R., "A Vortex in an Infinite Viscous Fluid," *Journal of Fluid Mechanics*, Vol. 11, No. 4, Cambridge University Press, London, England, Dec. **1961**, pp. 611–623.

Ludlum, F. H., "Severe Local Storms: A Review," *Meteorological Monographs*, Vol. 5, No. 27, American Meteorological Society, Boston, Mass., Sept. **1964**, pp. 1–32.

Malkus, Joanne Starr, and Witt, Georg, "The Evolution of a Convective Element: A Numerical Calculation," *The Atmosphere and the Sea in Motion*, Rockefeller Institute Press, New York, N.Y., **1959**, 509 pp. (see pp. 425–439).

Morton, B. R., "Model Experiments for Vortex Columns in the Atmosphere," *Nature*, Vol. 197, No. 4870, London, England, Mar. 2, **1963**, pp. 840–842.

Morton, B. R., Taylor, Geoffrey I., and Turner, J. S., "Turbulent Gravitational Convection From Maintained and Instantaneous Sources," *Proceedings of the Royal Society of London*, Ser. A, Vol. 234, No. 1196, England, Jan. 24, **1956**, pp. 1–23.

Nakagawa, Yoshinari, and Frenzen, Paul, "A Theoretical and Experimental Study of Cellular Convection in Rotating Fluids," *Tellus*, Vol. 7, No. 1, Stockholm, Sweden, Feb. **1955**, pp. 1–21.

National Physical Laboratories, "Modern Computing Methods," *Notes on Applied Science*, Second Edition, No. 16, London, England, 1962, 36–40.

Ogura, Yoshimitsu, "Convection of Isolated Masses of a Buoyant Fluid: A Numerical Calculation," *Journal of the Atmospheric Sciences*, Vol. 19, No. 6, Nov. **1962**, pp. 492–502.

Ogura, Yoshimitsu, "The Evolution of a Moist Convective Element in a Shallow, Conditionally Unstable Atmosphere: A Numerical Calculation," *Journal of the Atmospheric Sciences*, Vol. 20, No. 5, Sept. **1963**, pp. 407–424.

Ogura, Yoshimitsu, and Phillips, Norman A., "Scale Analysis of Deep and Shallow Convection in the Atmosphere," *Journal of the Atmospheric Sciences*, Vol. 19, No. 2, Mar. **1962**, pp. 173–179.

Richards, J. M., "Experiments on the Penetration of an Interface by Buoyant Thermals," *Journal of Fluid Mechanics*, Vol. 11, No. 3, Cambridge University Press, London, England, Nov. **1961**, pp. 369–384.

Turner, J. S., "Model Experiments Relating to Thermals With Increasing Buoyancy," *Quarterly Journal of the Royal Meteorological Society*, Vol. 89. No. 379, London, England, Jan. **1963**, pp. 62–74.

Turner, J. S., and Lilly, Douglas K., "The Carbonated-Water Tornado Vortex," *Journal of the Atmospheric Sciences*, Vol. 20, No. 5, Sept. **1963**, pp. 468–471.

Veronis, George, "Cellular Convection With Finite Amplitude in a Rotating Fluid," *Journal of Fluid Mechanics*, Vol. 5, No. 3, Cambridge University Press, London, England, Apr. **1959**, pp. 401–435.

Warner, J., and Telford, J. W., "Convection Below Cloud Base," *Journal of the Atmospheric Sciences*, Vol. 24, No. 4, July **1967**, pp. 374–382.

Wilkins, Eugene M., Sasaki, Yoshikazu, Friday, Elbert W., Jr., McCarthy, John, and McIntyre, James R., "Properties of Simulated Thermals in a Rotating Fluid," *Journal of Geophysical Research, Oceans and Atmospheres*, Vol. 74, No. 18, Aug. 20, **1969**, pp. 4472–4486.

Wilkins, Eugene M., Sasaki, Yoshikazu, and Schauss, Roger H., "Interactions Between the Velocity Fields of Successive Thermals," *Monthly Weather Review*, Vol. 99, No. 3, Mar. **1971**, pp. 215–226.

Williams, Dansy T., "A Report of the Kinematic Properties of Certain Small-Scale Systems," *NSSP Report* No. 11, National Severe Storms Project, U.S. Weather Bureau, Kansas City, Mo., Oct. **1962**, 22 pp.

Woodward, Betsy, "The Motion in and Around Isolated Thermals," *Quarterly Journal of the Royal Meteorological Society*, Vol. 85, No. 364, London, England, Apr. **1959**, pp. 144–151.

[*Received July 6, 1970; revised February 1, 1971*]